

PCCP

Accepted Manuscript



This is an *Accepted Manuscript*, which has been through the Royal Society of Chemistry peer review process and has been accepted for publication.

Accepted Manuscripts are published online shortly after acceptance, before technical editing, formatting and proof reading. Using this free service, authors can make their results available to the community, in citable form, before we publish the edited article. We will replace this *Accepted Manuscript* with the edited and formatted *Advance Article* as soon as it is available.

You can find more information about *Accepted Manuscripts* in the [Information for Authors](#).

Please note that technical editing may introduce minor changes to the text and/or graphics, which may alter content. The journal's standard [Terms & Conditions](#) and the [Ethical guidelines](#) still apply. In no event shall the Royal Society of Chemistry be held responsible for any errors or omissions in this *Accepted Manuscript* or any consequences arising from the use of any information it contains.

ARTICLE

Crystallographic dependence of photocatalytic activity for WO₃ thin films prepared by molecular beam epitaxy

Cite this: DOI: 10.1039/x0xx00000x

Guoqiang Li,^{a,b} Tamas Varga,^c Pengfei Yan,^c Zhiguo Wang,^{d*} Chongmin Wang,^c Scott A. Chambers,^a and Yingge Du^{c*}Received 00th January 2012,
Accepted 00th January 2012

DOI: 10.1039/x0xx00000x

www.rsc.org/

We investigate the impact of crystallographic orientation on the photocatalytic activity of single crystalline WO₃ thin films prepared by molecular beam epitaxy on the photodegradation of rhodamine B (RhB). A clear effect is observed, with (111) being the most reactive surface, followed by (110) and (001). Photoreactivity is directly correlated with surface free energy calculated by density functional theory calculations. The RhB photodegradation mechanism is found to involve hydroxyl radicals in solution formed from photo-generated holes and differs from previous studies performed on nanoparticles and composites.

Introduction

Heterogeneous photocatalysis using oxide semiconductors has many potential applications in energy production and environment remediation.¹⁻³ Better understanding of the mechanisms of photocatalytic reactions and the identification of more effective photocatalysts are key to advancing these novel technologies. Because most of the catalytic reactions occur on surfaces, it is crucial to understand and control the surface structure and associated properties in order to design better photocatalysts. The ability to synthesize crystalline photocatalysts with well-defined crystallographic orientations allows fundamental comparative studies to be carried out, which in turn help establish defensible relationships between surface atomic structures and photochemical properties.⁴⁻⁶ Photocatalysts in the forms of nanoparticles and thin films have been synthesized for this purpose. These include nanoparticles of TiO₂ samples with preferentially exposed (001) or (101) crystal planes,^{5, 7} ZnO(001),⁸ BiVO₄ nanosheets mainly consisting of {100} orientations,⁹ Ag₃PO₄ dodecahedrons with only {110} facets exposed and cubes bounded entirely by {100} facets,¹⁰ and WO₃ nanocrystals with {110} and {111} facets exposed^{11, 12}. These studies show that some facets have higher activities than others. It should be noted that all the nanoparticle samples contain at least two different exposed faces and the photodegradation mechanism may involve electron transfer from one surface to the other.¹³ In contrast, single-orientation thin film samples have been prepared and investigated to better elucidate the activity of specific crystal

planes.¹⁴⁻¹⁷ For example, rutile TiO_{2-x}N_x(110) and anatase TiO_{2-x}N_x(001) thin films prepared by molecular beam epitaxy (MBE),⁶ as well as NaNbO₃, NiO and ZnO thin films prepared by pulsed laser deposition (PLD) have been used to investigate the crystallographic dependence of their photocatalytic activities.¹⁵⁻¹⁷

Tungsten trioxide (WO₃) has been demonstrated to split water and degrade a wide range of organic compounds and is one of the most widely studied photocatalysts.¹⁸⁻²⁰ Many modifications have been made to improve its photocatalytic and photoelectrochemical performance, including noble metal loading,^{21, 22} nanoparticle synthesis,^{9, 23-25} and hydrogen treatment.^{26, 27} However, the crystallographic orientation dependence of its photocatalytic activity has not been established or systematically studied. In earlier work, nano- or micro-scale crystals of WO₃·xH₂O with special morphology and specific crystal facets exposed were prepared by chemical synthesis.^{11, 12, 28} Li *et al.*¹² found that the degree of exposure of (010) facets in orthorhombic WO₃·xH₂O samples correlates well with measured photocatalytic activities. Shi *et al.*¹¹ reported that octahedral WO₃·xH₂O with (111) facets exposed possesses the highest photocatalytic activities for methylene blue degradation. Zhang *et al.*²⁸ reported that orthorhombic WO₃ nanocrystals with a high percentage of (001)-facet exposure exhibit a higher activity for rhodamine B (RhB) degradation. WO₃ crystals are generally formed from corner and edge sharing of WO₆ octahedra. The phases with corner sharing include monoclinic I (γ-WO₃), monoclinic II (ε-WO₃),

triclinic (δ -WO₃), orthorhombic (β -WO₃), tetragonal (α -WO₃), and cubic WO₃.¹⁸ It has been shown that epitaxial interface formation can stabilize certain phases that are otherwise unstable. Specifically, single-crystal WO₃ films with cubic or tetragonal structures can be grown on nearly lattice matched perovskite substrates, such as LaAlO₃ (LAO) and SrTiO₃.²⁹⁻³²

In this study, (001), (110), and (111)-oriented WO₃ single crystalline films were grown on LAO substrates with the same orientations. Their photocatalytic activities were evaluated using the RhB degradation under UV-visible light irradiation. The photocatalytic activity was found to increase in going from (001) to (110) to (111). Density functional theory (DFT) calculations show that the surface energy increases in the same order, which may explain the anisotropic photocatalytic activity. Through controlled studies, the photodegradation of RhB on WO₃ is determined to be caused primarily by hydroxyl radicals in solution which form from photo-generated holes.

Experimental

Materials and methods

WO₃ thin films were grown in a customized MBE system which has been described elsewhere.³³ High-purity WO₃ powder (Sigma-Aldrich, >99.99%) was evaporated from a high-temperature effusion cell at a film growth rate of ~ 0.2 Å/s as calibrated by a quartz crystal microbalance. The LAO substrates (10×10×0.5 mm, MTI Corporation) substrate temperature was set to 500°C and an activated oxygen beam (with O₂ partial pressure in the chamber set at $\sim 3 \times 10^{-6}$ Torr) was incident on the sample during deposition to prevent sample reduction. WO₃ films of thickness ~ 90 nm were grown on (001), (110) and (111) oriented LAO substrates. The three substrates were mounted on a 2" holder, and the holder was rotated at 1 rpm during the deposition to ensure composition and thickness uniformity. The as-grown films were found to be fully stoichiometric as revealed by *in-situ* x-ray photoelectron spectroscopy (XPS).³¹ Epitaxial relationship, crystalline quality, and lattice parameters were investigated using high-resolution X-ray diffraction (XRD) with a Philips X'Pert Materials Research diffractometer (MRD) equipped with a fixed Cu anode operating at 45 kV and 40 mA. A hybrid monochromator, consisting of four-bounce double-crystal Ge (220) and a Cu X-ray mirror, was placed in the incident beam path to generate monochromatic Cu K α X-rays ($\lambda = 1.54056$ Å) with a beam divergence of 12 arc seconds. For scanning transmission electron microscopy (S/TEM) imaging, an FEI Titan 80-300 microscope equipped with a probe forming lens corrector was used. To avoid ion and electron beam damage to the WO₃ film, we prepared the TEM samples by mechanical thinning followed by Ar ion sputtering at low energy.

The photocatalytic activities of the as-prepared films were evaluated using the RhB photodegradation reaction under UV-visible light irradiation of 300-W Hg-Xe lamp (Newport Co Ltd, USA) with a cut-off filter of 305 nm. The photocatalytic reaction was carried out in a sealed quartz cuvette with 1 ml

RhB solution and a path length of ~ 5 mm. No stirring was done during irradiation, but the cuvette was shaken before the absorbance was measured. The initial concentration of RhB solution was 2.5 mg L⁻¹. After 10 minutes of reaction equilibration in the dark, the change in RhB absorbance was recorded *in-situ* at 10 min intervals using a UV-Vis spectrophotometer (Cary 5000, Agilent, USA). In some controlled experiments, the isopropanol (IPA) or methanol was added.

Calculation

We used DFT to calculate the surface free energies of WO₃(001), (110), and (111). All calculations were performed using a linear combination of numerical localized atomic orbital basis sets for the description of valence electrons as implemented in the SIESTA code.³⁴ This formalism utilizes norm-conserving nonlocal pseudopotentials for the atomic cores.³⁵ The projector augmented wave (PAW) method was used to describe electron-ion interaction,³⁶ while the generalized gradient approximation using the Perdew-Burke-Ernzerhof (PBE) functional was used to describe the electron exchange-correlation. The valence electrons were taken to be 2s²2p⁴ for O and 6s²5d⁴ for W, respectively. The valence electron wave functions were expanded using a double- ζ basis set. The convergences with respect to basis set, the cut off energy, and the k point mesh have been tested and the cutoff energy and the k-points mesh used in this work are appropriate for the system.

The WO₃(001) and (110) surfaces consist of terminations containing both W and O whereas the WO₃(111) surface consists of a purely W termination. All three planes could also be terminated with a pure O plane (not shown), and these structures were also considered. The periodic boundary condition was used in our slab calculations. For the terminations we considered, the slabs are separated by at least 25 Å of vacuum. During surface structure optimization, all atoms are fully relaxed. The cleavage energy of surface $E_{cl}(\text{O}+\text{WO})$ was calculated from the total energy computed for the unrelaxed slabs using the formula

$$E_{cl}(\text{O} + \text{WO}) = \frac{1}{4S} [E_{slab}^{unrel}(\text{O}) + E_{slab}^{unrel}(\text{WO}) - nE_{bulk}] \quad (1)$$

where S is the area of the surface, E_{slab}^{unrel} is the total energy of unrelaxed slab, E_{bulk} is the bulk energy per formula unit in the cubic structure, n is the total number of bulk formula units in the two slabs, and the factor of 1/4 accounts for the fact that four surfaces are created upon the crystal cleavage.

When both surfaces of the slab are allowed to relax, the relaxation energies for each of the surfaces is given by

$$E_{rel} = \frac{1}{2S} [E_{slab}^{rel} + E_{slab}^{unrel}] \quad (2)$$

where S is the area of the surface, E_{slab}^{rel} is the terminated slab energy after relaxation and the factor of 1/2 enters because two surfaces are created upon crystal cleavage. The surface energy is calculated by³⁷

$$E_{surf} = E_{rel} + E_{cl} \quad (3)$$

The W atoms move inward after relaxation for the W-terminated (111) surface so the W-terminated (111) surface changes to a mixed WO-termination.

Results and discussion

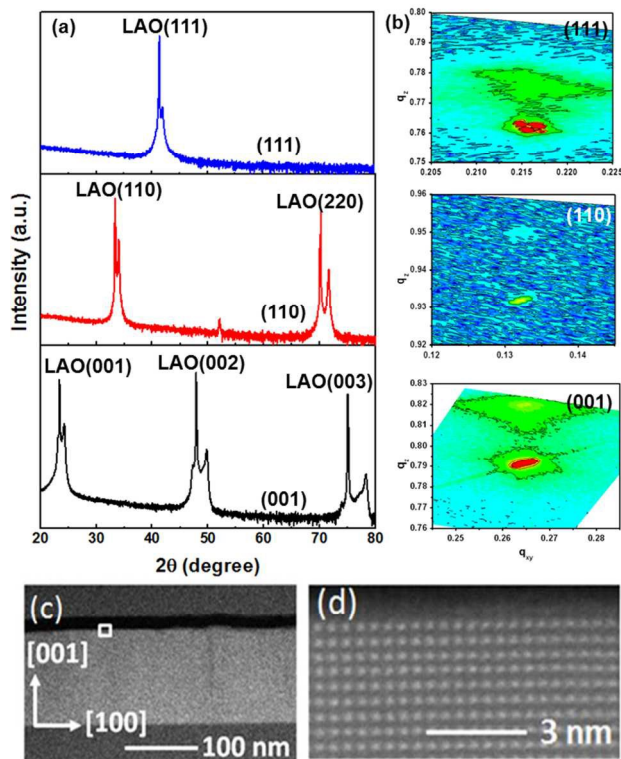


Fig. 1 (a) X-ray diffraction θ - 2θ scans for 90 nm WO_3 films on LaAlO_3 (111), (110), and (001), respectively. (b) Reciprocal space maps near the (122), (321), and (103) Bragg reflection of LAO for (111), (110), and (001) oriented WO_3 films, respectively, showing the films are strained to the substrate in-plane. (c) Scanning transmission electron microscopy image of a 150 nm WO_3 (001) film. A magnified view of the film/vacuum interface marked by square in (c) is displayed in (d).

The XRD results for the 90 nm film are shown in Fig. 1a. A single film peak adjacent to the sharper substrate (001), (110) and (111) peak was observed in the out-of-plane θ - 2θ scan for each orientation, confirming the epitaxial relationships $(001)_{\text{WO}_3} \parallel (001)_{\text{LAO}}$, $(110)_{\text{WO}_3} \parallel (110)_{\text{LAO}}$ and $(111)_{\text{WO}_3} \parallel (111)_{\text{LAO}}$. The lattice parameter of LAO is 3.796 Å. The out-of-plane lattice spacings were measured to be 3.66 Å for WO_3 (001), 2.63 Å for WO_3 (110) and 2.16 Å for WO_3 (111), close to the values expected for the bulk, cubic phase (3.70 Å, 2.62 Å, and 2.14 Å, respectively). In-plane reflections are consistent with a tetragonal structure, and the reciprocal space map (RSM) near the (103), (321) and (122) Bragg reflection of LAO shows the WO_3 (001) (110) and (111) films are largely coherently strained to the substrates, as shown in Fig. 1b. Scanning transmission electron microscopy (STEM) images for a 150 nm thick WO_3 (001) film reveal the surface is flat and doesn't facet, as seen in Fig. 1c. The region marked by a square in Fig. 1c is the film/vacuum interface, and the black color comes from the

carbon coating used to prepare TEM sample. Majority of the (001) surface is composed of flat terraces separated by monoatomic steps. A magnified view of the square region shown in Fig. 1d reveals the high crystallographic quality and atomic flatness of the (001) surface.

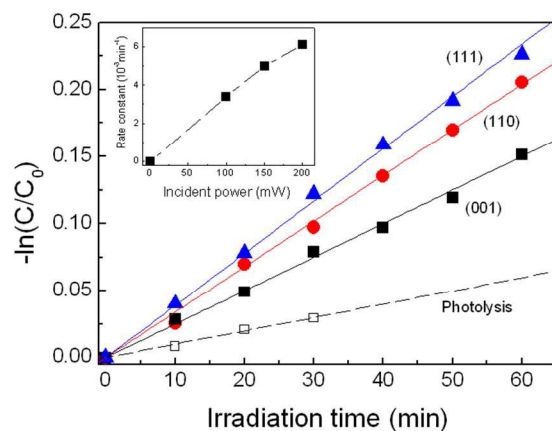


Fig. 2 Plot of $-\ln(C/C_0)$ vs. irradiation time over WO_3 (001), (110) and (111) films under UV-visible light irradiation. The inset is rate constant as a function of incident light power obtained from WO_3 (110).

The RhB degradation curves for all three WO_3 thin films can be fit to simple first-order reaction kinetics, i.e., $dC/dt = kC$, or $-\ln(C/C_0) = kt$, where C and C_0 are the RhB concentration after t min light irradiation and the initial concentration, respectively, and k is the apparent rate constant for photodegradation. We also investigated the reaction rate as a function of the incident power, as an essential qualification for photocatalytic reaction is that the reaction rate must depend on the light intensity.³⁸ The rate constant increases linearly with incident light intensity, as shown in the inset of Fig. 2. This observation shows that the reaction is a typical photocatalytic degradation induced by light absorption.

The photocatalytic activities for RhB degradation under UV-visible light irradiation over WO_3 (001), (110) and (111) are displayed in Fig. 2. As a control, the RhB photolysis process in the absence of a WO_3 surface was also monitored under the same conditions. The rate constants are $2.5 \times 10^{-3} \text{ min}^{-1}$ for WO_3 (001), $3.4 \times 10^{-3} \text{ min}^{-1}$ for WO_3 (110), and $3.9 \times 10^{-3} \text{ min}^{-1}$ for WO_3 (111), respectively, all much higher than the homogeneous photolysis rate constant, $1 \times 10^{-3} \text{ min}^{-1}$.

As discussed above, it is known for several material systems that different crystallographic orientations exhibit different photocatalytic activities. Surface free energy is frequently considered as an important factor in determining the more reactive crystallographic facets.^{10, 16} Therefore, we used DFT to calculate the surface free energies of WO_3 (001), (110), and (111).

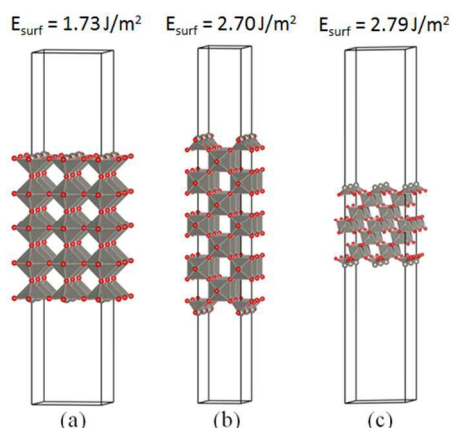


Fig. 3 (a) (001) and (b) (110) surfaces of cubic WO_3 terminated with W (grey spheres) and O (red spheres), and (c) (111) surface terminated with purely W.

The $\text{WO}_3(001)$ and (110) surfaces consist of terminations containing both W and O whereas the $\text{WO}_3(111)$ surface consists of a purely W termination, as shown in Fig. 3. The calculated surface energy for the WO terminated (001) surface is 1.73 J/m^2 , which agrees well with another DFT result, 1.74 J/m^2 ³⁹, but is slightly higher than $1.39\text{--}1.67 \text{ J/m}^2$, the values for the reconstructed $\text{WO}_3(001)$ surface calculated by interatomic potentials.⁴⁰ The calculated surface energy is 2.70 J/m^2 for (110), and 2.79 J/m^2 for (111). It can be seen that the surface energy increases in going from (001) to (110) to (111) for the W-containing terminations. The similar trend was also found for the purely O-terminated surfaces ($2.21, 3.63, \text{ and } 4.78 \text{ J/m}^2$ for the (001), (110) and (111), respectively). The surface energy for O-terminated (111) surface agrees well with the value of 4.89 J/m^2 predicted by Oliver *et al.*⁴⁰ using the METADISE code. For the three orientations investigated, the photocatalytic activities correlate with the surface energy, i.e., the larger the surface energy, the higher the photocatalytic activity. Surface free energy has a direct impact on defect formation and surface wetting properties, which may contribute to the differences observed in the photocatalytic activity.

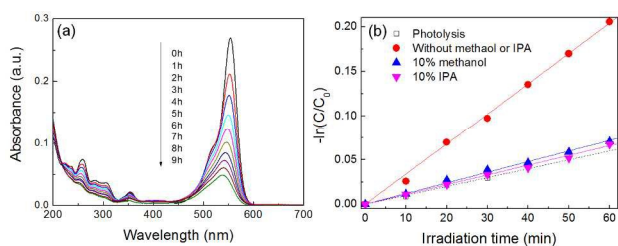


Fig. 4 (a) Temporal UV-visible absorption spectral changes for the RhB solution in contact with a $\text{WO}_3(110)$ film as a function of irradiation time. (b) Plot of $-\ln(C/C_0)$ vs. irradiation time with and without scavengers.

To identify the mechanism of RhB degradation over WO_3 thin films, the (110) film was exposed for 9 hrs with absorption spectra measured every hour. The results are shown in Fig. 4a. The RhB degradation is a complex process where two different sets of spectral changes could be observed in the UV-visible absorption spectra of RhB associated with two different

mechanisms.⁴¹ One is that the absorbance of the main peak would decrease and be accompanied by a change in the maximum absorption wavelength from 554 to 499 nm. This change would be accompanied by the appearance of new peaks between 200 and 300 nm, indicating the apparent deethylation of RhB. The second is that the absorbance of the main peak would decrease, with little change in the maximum absorption wavelength, and no new peaks appear between 200 and 300 nm. This spectral change would reveal cleavage of the entire chromophore structure (cycloreversion).⁴¹ As shown in Fig. 4a, the absorbance at 554 nm decreases significantly with increasing irradiation time, the change in the maximum absorption wavelength is relatively small, and no new absorption peaks are detected. Thus, RhB cleavage is the dominate process.

To gain more insight into the reaction path involved in the photodegradation of RhB, the effects of molecular scavengers were considered. IPA has been described as a hydroxyl radical quencher because of its vigorous reaction with $\bullet\text{OH}$ radicals.^{42, 43} To test for the importance of $\bullet\text{OH}$ radicals, 10% (by volume) IPA was added to the RhB solution and the experiment was repeated. Extensive suppression of the RhB degradation process was observed, as shown in Fig. 4b. The rate constant with IPA is $1.1 \times 10^{-3} \text{ min}^{-1}$, which is much smaller than that without IPA ($3.4 \times 10^{-3} \text{ min}^{-1}$) but similar to the photolysis rate constant, $1.0 \times 10^{-3} \text{ min}^{-1}$. This result reveals that $\bullet\text{OH}$ radicals play a dominant role in the reaction mechanism of RhB oxidation on WO_3 surfaces.

$\bullet\text{OH}$ radicals can be formed via two different pathways: electron-transfer mediation and photo-generated hole reaction. It is known that electron-hole pairs are generated by light excitation in semiconductor photocatalysts. These carriers then diffuse to the surface and drive the photocatalytic reaction. To clarify the reaction pathway of $\bullet\text{OH}$ radicals generated over WO_3 films, we added methanol to the RhB solution to study its effect as a hole scavenger.^{41,44} After addition of 10%-by-volume methanol to the RhB solution, a remarkable suppress effect was observed. The rate constant with methanol is $1.2 \times 10^{-3} \text{ min}^{-1}$, which is very close to the photolysis rate constant, $1.0 \times 10^{-3} \text{ min}^{-1}$. The result suggests that photogenerated holes play a dominant role in the formation of hydroxyl radicals. Previous studies using scavengers indicated that the active species, O_2^- and h^+ over WO_3 nanoparticles and composites, play a major role in the photocatalytic degradation of RhB, but $\bullet\text{OH}$ does not play a major role.^{25, 43, 45} However, our results indicate that the hydroxyl radicals generated from holes are indeed the dominate species. This difference might come from the different approaches required to prepare the samples. Compared to our single-crystalline thin film samples prepared by MBE, WO_3 nanoparticles and composite exhibit multiple crystallographic orientations, grain boundaries, surface defects and impurities. These could have a significant impact on the reaction pathways, reaction intermediates, and hence the experimental observations.¹⁴

Conclusions

In summary, we have investigated the photocatalytic activity of WO₃ single crystal thin films with (001), (110) and (111) orientations. The catalytic activity was found to depend strongly on crystallographic orientation. The surface photoreactivity increases in going from (001) to (110) to (111), as does the surface free energy. The photocatalytic degradation of RhB over WO₃(110) is driven by hydroxyl radicals in solution, which form from photo-generated holes.

Acknowledgements

A portion of the work was supported by the U.S. Department of Energy, Office of Basic Energy Sciences, Division of Materials Sciences and Engineering under Award 10122. YD acknowledges support by EMSL's Intramural Research and Capability Development Program. GL acknowledges support by Henan University, China and National Natural Science Foundation of China (21103041). The work was performed at the W. R. Wiley Environmental Molecular Sciences Laboratory, a DOE User Facility sponsored by the Office of Biological and Environmental Research. The authors thank Z. Dohnalek and T. Kaspar for insightful discussions and help in proofreading the final manuscript.

Notes and references

^a Fundamental & Computational Sciences Directorate, Pacific Northwest National Laboratory, Richland, Washington 99352, USA

^b Key Laboratory of Photovoltaic Materials of Henan Province, School of Physics & Electronics, Henan University, Kaifeng 475004, P.R. China

^c Environmental Molecular Sciences Laboratory, Pacific Northwest National Laboratory, Richland, Washington 99352, USA. E-mail: yingge.du@pnnl.gov

^d Department of Applied Physics, University of Electronic Science and Technology of China, Chengdu, 610054, P. R. China. E-mail: zgwang@uestc.edu.cn

- H. Kisch, *Angew. Chem. Int. Ed.*, 2013, **52**, 812-847.
- H. Tong, S. Ouyang, Y. Bi, N. Umezawa, M. Oshikiri and J. Ye, *Adv. Mater.*, 2012, **24**, 229-251.
- N. Serpone and A. V. Emeline, *J. Phys. Chem. Lett.*, 2012, **3**, 673-677.
- L. Chen, Z. J. Li, R. S. Smith, B. D. Kay and Z. Dohnalek, *J. Am. Chem. Soc.*, 2014, **136**, 5559-5562.
- H. G. Yang, C. H. Sun, S. Z. Qiao, J. Zou, G. Liu, S. C. Smith, H. M. Cheng and G. Q. Lu, *Nature*, 2008, **453**, 638-U634.
- T. Ohsawa, I. Lyubintsky, Y. Du, M. A. Henderson, V. Shutthanandan and S. A. Chambers, *Phys. Rev. B*, 2009, **79**.
- X. Wang, R. G. Li, Q. Xu, H. X. Han and C. Li, *Acta Phys-Chim Sin*, 2013, **29**, 1566-1571.
- A. McLaren, T. Valdes-Solis, G. Q. Li and S. C. Tsang, *J. Am. Chem. Soc.*, 2009, **131**, 12540-12541.
- G. C. Xi and J. H. Ye, *Chem. Commun.*, 2010, **46**, 1893-1895.
- Y. Bi, S. Ouyang, N. Umezawa, J. Cao and J. Ye, *J. Am. Chem. Soc.*, 2011, **133**, 6490-6492.
- J. C. Shi, G. J. Hu, R. Cong, H. J. Bu and N. Dai, *New J. Chem.*, 2013, **37**, 1538-1544.
- J. Y. Li, J. F. Huang, J. P. Wu, L. Y. Cao, Q. J. Li and K. Yanagisawa, *Crystengcomm*, 2013, **15**, 7904-7913.
- T. Tachikawa and T. Majima, *J. Am. Chem. Soc.*, 2009, **131**, 8485-8495.
- S. A. Chambers, *Adv. Mater.*, 2010, **22**, 219-248.
- G. Q. Li, Z. G. Yi, Y. Bai, W. F. Zhang and H. T. Zhang, *Dalton T.*, 2012, **41**, 10194-10198.
- G. Q. Li, Z. G. Yi, H. T. Wang, C. H. Jia and W. F. Zhang, *Appl. Catal. B: Environ.*, 2014, **158-159**, 280-285.
- Y. Wang, F. Zhang, L. Wei, G. Li and W. Zhang, *Physica B: Condensed Matter*, 2015, **457**, 194-197.
- H. Zheng, J. Z. Ou, M. S. Strano, R. B. Kaner, A. Mitchell and K. Kalantar-zadeh, *Adv. Funct. Mater.*, 2011, **21**, 2175-2196.
- G. Xi, J. Ye, Q. Ma, N. Su, H. Bai and C. Wang, *J. Am. Chem. Soc.*, 2012, **134**, 6508-6511.
- J. G. Yu, L. F. Qi, B. Cheng and X. F. Zhao, *J. Hazard. Mater.*, 2008, **160**, 621-628.
- A. Tanaka, K. Hashimoto and H. Kominami, *J. Am. Chem. Soc.*, 2014, **136**, 586-589.
- R. Abe, H. Takami, N. Murakami and B. Ohtani, *J. Am. Chem. Soc.*, 2008, **130**, 7780-7781.
- D. Chen and J. Ye, *Adv. Funct. Mater.*, 2008, **18**, 1922-1928.
- D. Chen, L. Gao, A. Yasumori, K. Kuroda and Y. Sugahara, *Small*, 2008, **4**, 1813-1822.
- Y. Zheng, G. Chen, Y. G. Yu, Y. Wang, J. X. Sun, H. M. Xu and Y. S. Zhou, *New J. Chem.*, 2014, **38**, 3071-3077.
- G. M. Wang, Y. C. Ling, H. Y. Wang, X. Y. Yang, C. C. Wang, J. Z. Zhang and Y. Li, *Energy & Environ. Sci.*, 2012, **5**, 6180-6187.
- G. Liu, J. F. Han, X. Zhou, L. Huang, F. X. Zhang, X. L. Wang, C. M. Ding, X. J. Zheng, H. X. Han and C. Li, *J. Catal.*, 2013, **307**, 148-152.
- D. Q. Zhang, S. L. Wang, J. Zhu, H. X. Li and Y. F. Lu, *Appl. Catal. B: Environ.*, 2012, **123**, 398-404.
- A. Garg, J. A. Leake and Z. H. Barber, *J. Phys D Appl. Phys.*, 2000, **33**, 1048-1053.
- P. Tagtstrom and U. Jansson, *Thin Solid Films*, 1999, **352**, 107-113.
- Y. Du, K. H. L. Zhang, T. Varga and S. A. Chambers, *Appl. Phys. Lett.*, 2014, **105**, 051606.
- Y. G. Du, M. Gu, T. Varga, C. M. Wang, M. E. Bowden and S. A. Chambers, *ACS Appl. Mater. & Interfaces*, 2014, **6**, 14253-14258.
- K. H. L. Zhang, P. V. Sushko, R. Colby, Y. Du, M. E. Bowden and A. Chambers, *Nat. Commun.*, 2014, **5**.
- J. M. Soler, E. Artacho, J. D. Gale, A. Garcia, J. Junquera, P. Ordejon and D. Sanchez-Portal, *J. Phys.-Condes. Matter*, 2002, **14**, 2745-2779.
- N. Troullier and J. L. Martins, *Phys. Rev. B*, 1991, **43**, 1993-2006.
- G. Kresse and D. Joubert, *Phys. Rev. B*, 1999, **59**, 1758-1775.
- J. Cui and W. Liu, *Physica B: Condensed Matter*, 2010, **405**, 4687-4690.
- L. B. Liao, Q. H. Zhang, Z. H. Su, Z. Z. Zhao, Y. N. Wang, Y. Li, X. X. Lu, D. G. Wei, G. Y. Feng, Q. K. Yu, X. J. Cai, J. M. Zhao, Z. F. Ren, H. Fang, F. Robles-Hernandez, S. Baldelli and J. M. Bao, *Nat. Nanotechnol.*, 2014, **9**, 69-73.

39. D. Zhang, S. Wang, J. Zhu, H. Li and Y. Lu, *Appl. Catal. B: Environ.*, 2012, **123–124**, 398–404.
40. P. M. Oliver, S. C. Parker, R. G. Egdell and F. H. Jones, *J. Chem. Soc. Faraday T.*, 1996, **92**, 2049–2056.
41. J. D. Zhuang, W. X. Dai, Q. F. Tian, Z. H. Li, L. Y. Xie, J. X. Wang, P. Liu, X. C. Shi and D. H. Wang, *Langmuir*, 2010, **26**, 9686–9694.
42. Y. Park, Y. Na, D. Pradhan, B.-K. Min and Y. Sohn, *Crystengcomm*, 2014, **16**, 3155.
43. J. Cao, B. D. Luo, H. L. Lin, B. Y. Xu and S. F. Chen, *Appl. Catal. B: Environ.*, 2012, **111**, 288–296.
44. Y. Zheng, G. Chen, Y. G. Yu, J. X. Sun, Y. S. Zhou and J. Pei, *Crystengcomm*, 2014, **16**, 6107–6113.
45. K. Jothivenkatachalam, S. Prabhu, A. Nithya and K. Jeganathan, *Rsc Adv.*, 2014, **4**, 21221–21229.